Available online at www.CivileJournal.org

Civil Engineering Journal

Vol. 5, No. 6, June, 2019

Experimental Investigation for Non and Partially Composite Cold-Formed Steel Floor Beams

Tuka Mohammed Qasim [a*], Salah Rohaima Al-Zaidee [b]

[a] *M.Sc. Student, College of Engineering-University of Baghdad, Baghdad, Iraq.*

[b] *Assistant Professor, College of Engineering-University of Baghdad, Baghdad, Iraq.*

Received 18 February 2019; Accepted 06 May 2019

Abstract

In this study, six full-scaled models of RC floors supported by cold-form steel sections have been tested. Each model consists of RC 75mm thick slab supported on two parallel cold-formed steel beams with a span of 3m and spacing of 500mm. The slab has an overhang part of 250mm on each side. In the first and fourth models, the slab has been casted directly on the top flanges with no shear connector to simulate the effectiveness of friction in resisting of the lateral-torsional buckling. Shear studs have been drilled in the second and fifth models to ensure the composite action. Finally, the flanges have been embedded for the third and sixth models. A single channel beam is used in the first, second, and third models while a built-up beam is used in the fourth, fifth, and sixth models. Each model has been loaded up to failure under a pure bending with two-line loads located at the third points. Data for loads, deformations, and strains have been gathered. Except the fourth and the sixth models that failed in local buckling modes, all other models failed in global lateral-torsional buckling modes. For the single beam models; the load carrying capacity of the non-composite model is 82.9% less than the capacity of the composite models with shear studs and embedded flange. For the built-up models; the load carrying capacity of the non-composite model is 44.2 % less than the loads of the composite model with shear stud and 48.7% less than the model with the embedded flange.

Keywords: Cold-Formed Steel; Floor Beam, Experimental; Lateral-Torsional Buckling; Noncompsite Action; Composite Action.

1. Introduction

During the last few decades the using of the Cold-formed steel beams has increased significantly where they have been utilized as floor beams. Since the cold-formed steel members are a relatively thin with respect to their width and have mono-symmetric or unsymmetric cross-sections, they may buckle at stress value lower than the yield stress when subjected to compression or bending. Lateral-torsional buckling behavior of the cold formed steel members is more complicated than that of the hot-rolled sections. Experimental tests of simply supported laterally unbraced cold-formed beams was executed in 1998 by Put et al [1]. At the same time, Pi et al. [2] provided a numerical investigation using an advanced finite-element model to study the elastic lateral-torsional buckling and inelastic strengths of the cold-formed steel beams to improved design rules.

In 2012 N. D. Kankanamge and M. Mahendran developed a finite element model using ABAQUS. The model has been verified using available numerical and experimental results and subsequently it has been used to study the behavior and design of cold-formed steel beams subject to lateral–torsional buckling [3]. M. Anbarasu dealt with the ultimate

* Corresponding author: tukam26@gimal.com

http://dx.doi.org/10.28991/cej-2019-03091341

strength, post-buckling behavior and design of cold-formed steel lipped channel beams affected by local-distortional buckling mode interaction and subjected to uniform bending about the major axis in 2016 [4]. An experimental and numerical investigation of cold-formed steel built-up beams with different screw arrangements has been presented in 2018 by L. Wang and B. Young [5]. A pioneering concept has been presented by N. Hadjipantelis [6] to enhance the load-carrying capacity and serviceability performance of cold-formed steel beams with utilizing prestressing techniques.

Use of cold-formed steel sections as composite joists in floor systems is limited in the previous studies in spite of its advantages in reducing slab thickness and flexibility of the system. The main problem in application of the designs is ensuring adequate shear transfer between the concrete slab and the cold-formed beam section, whose thickness is often too small for welding of conventional shear studs. A. Hanaor in 2000 [7] and B. S. Lakkavalli and Y. Liu in 2006 [8] studied the behaviour and capacity of composite slab joists consisting of cold-formed steel C-sections and concrete using four shear mechanics. Results indicate that in most cases, design of shear connectors can conservatively be based on codes of practice for the design of cold-formed connections, full-scale tests indicate high ductility and capacity which exceeds design assumptions. An experimental results of a vibration characteristics of cold-formed steel-supported lightweight residential floor systems is carried by L. Xu and F. M. Tangorra in 2006 [9].

The use of cold-formed steel beams in conjunction with wood-based flooring panels for the construction of lightweight and economical flooring systems is widespread. P. Kyvelou et al proposed an experimental investigations in 2017 showed the degree of composite action that can arise between cold-formed steel joists and wood-based flooring panel [10] and [11]. In 2018 P. Kyvelou et al presented a numerical investigation into the degree of composite action that may be mobilized within floor systems comprising cold-formed steel joists and wood-based particle boards [12]. D. C. Fratamicoa et al (2018) studied experiments addressing the buckling and collapse behavior of common built-up cold-formed steel (CFS) columns [13]. By Krishanu Roya et al, forty experimental tests were conducted on back-to-back gapped built-up cold-formed steel channel-sections to cover the range of non-dimensional slenderness from short to slender columns. A nonlinear finite element model was then prepared to show a good agreement with the experimental results [14].

An experimental work on quick connecting systems alternative to screws was carried out by the European project ELISSA (Energy Efficient Lightweight-Sustainable-Safe-Steel Construction). Results for monotonic and cyclic shear tests were discussed by L.Firoino et al [15]. In 2018, five different types of mechanisms for members in compression with different eccentricities were examined by V. Ungureanu et al to investigates the possibility to use the local plastic mechanisms to characterize the ultimate strength of short thin-walled cold-formed steel members subjected to eccentric compression about the minor axis [16]. F. Cardoso et al in 2019 concerned the system reliability calibrations of a design-by-analysis method with a particular focus on cold-formed steel portal frames. A limit-state design criterion has been developed to be consistent with a desired level of system safety [17]. Ye Yao et al presents a finite element based method to predict residual stresses and equivalent plastic strains in cold-formed steel hollow sections [18].

In this paper, six full-scaled models of RC floors supported by cold-form steel sections with different connections between the concrete and the steel have been tested. It aims to study the behavior of the non and partially composite cold-formed floor beam and to show how connection mechanisms can affect the stiffness, strength, and stability of the cold-formed steel supporting beams.

2. Description the Elements and Models

Six floor systems full-scale models are the best approach to predict the behavior of non and partially composite cold-formed steel beams. Each one consists of concrete slab 3m by 1m reinforced with $\phi 10\ mm\ at\ 200\ mm$ rebar in both directions. This slab is supported on two cold-formed simply supported beams its dimensions is listed in Table 1. Two-line loads have been applied at the third points of specimens through a distribution beams to generate a pure bending region in the central third of the span. A jack with a capacity of 30 Ton has been used to apply the load and a dial gauge adopted to measure the mid-span deflection.

The first Model consists of two C-section beams; their flanges are in contact with concrete slab surface as shown in Figure 1. The aim of this model is to study the effectiveness of friction between the non-composite steel beams and concrete slab on the lateral restrained of these beams. In the second model, shear studs have been drilled to the beams top flange to have a composite action. The aim of this model was to see the role of the shear studs on the behavior of the cold formed steel beams. Top flanges have been embedded in the concrete slab in the third model. The main idea of this model was to show how the flange embedment in the concrete can affect the behavior. The fourth, fifth, and sixth models are respectively similar to the first, second, and third models but with double C built up beams.

Table 1. Beam dimensions

Average beam span (mm)	3002
Average flange width (mm)	59
Average web depth (mm)	208
Average beam thickness (mm)	1.9

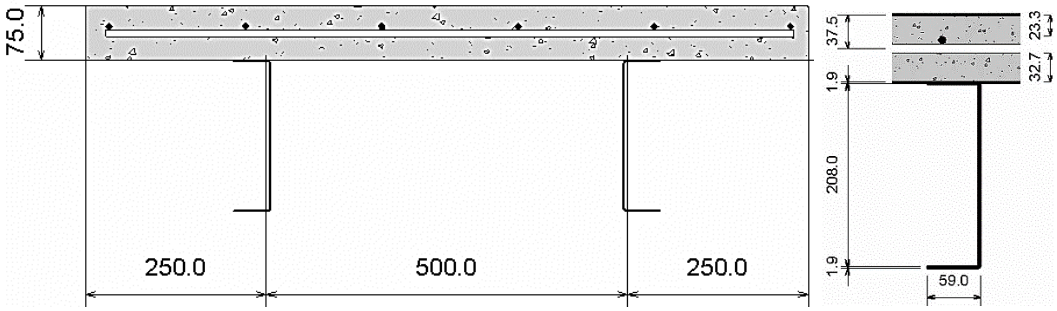

Figure 1. First model beams flange in contact with the concrete (single C-section)

3. Material Properties

To get essential information about material properties that have been used in construction of the models, the following tests have been executed.

3.1. Grading Test of Sand and Gravel

Two kilograms of sand and five kilograms of gravel have been tested in the laboratory. The results are presented in Table 2 and

Table 3 show that the gravel and the sand are within the limitation of Iraqi Standard Specification No.45. The gravel has a maximum size of aggregate of 12.5 mm.

Table 2. Result of sieving the gravel

Sieve opening diameter (mm)	Passing percentage
20	100
14	100
10	69
5	0.32

Table 3. Result of sieving the sand

Sieve opening diameter (mm)	Passing percentage
10	100.0
4.75	90.0
2.36	78.6
1.18	66.7
0.6	52.9
0.3	19.9
0.15	3.9

3.2. Tensile Test of Bars

Three ϕ 10 mm rebars of 0.5m length were tested in the Consultant Engineering Bureau laboratory. The results are listed in below

Table 4. Bars test values of specimens.

Specimen	Maximum elongation percentage	Yield stress (MPa)	Tensile stress(MPa)
1	13.2	548.03	644.33
2	14	555.41	651.72
3	13.5	531.72	629.68

3.3. Coupon Test of Cold-Formed Steel

The mechanical properties of the cold-formed steel (CFS) channel sections were evaluated based on tensile coupon tests. The coupons were cut along the longitudinal direction of channel sections. The standard flat coupons were dimensioned according to the guidelines provided by the ASTM Standards A370-03, "Standard Test Methods and

Definitions for Mechanical Testing of Steel Products", [19]. The test was done in the consulting engineering bureau of university of Baghdad and the result is listed below:

- Yield Stress =344.12 Mpa
- Tensile Stress=426.46 Mpa

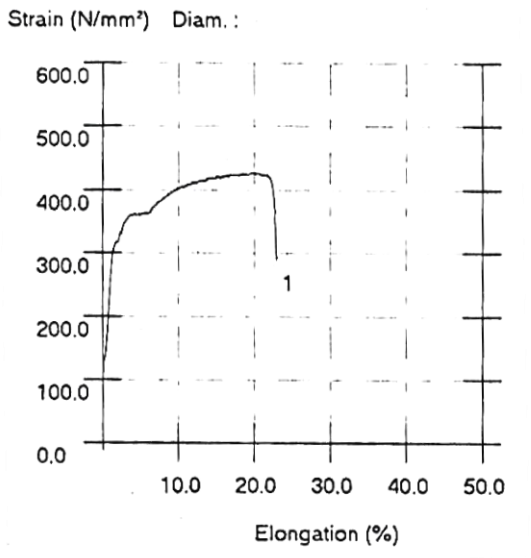

Figure 2. Coupon test results

4. Preparation of Models before Casting

In the models that have a single channel beams, the channels were braced at their ends using U shape steel bars, for the models with double C built up beams the built-up I-sections fabricated by connecting two C-sections back-to-back using two rows of $\phi 10mm$ bolts drilled along its length and fasten with nets. First row was drilled 50mm below the top flange while the second row was at 100 mm below the first one, see Figure 3. A spacing of 300mm center to center between the bolts has been adopted in the two rows. As indicated in Figure 4, two timber block with dimensions $202 \times 60 \times 30\ mm$ have been drilled to the end of each beam to prevent web crippling.

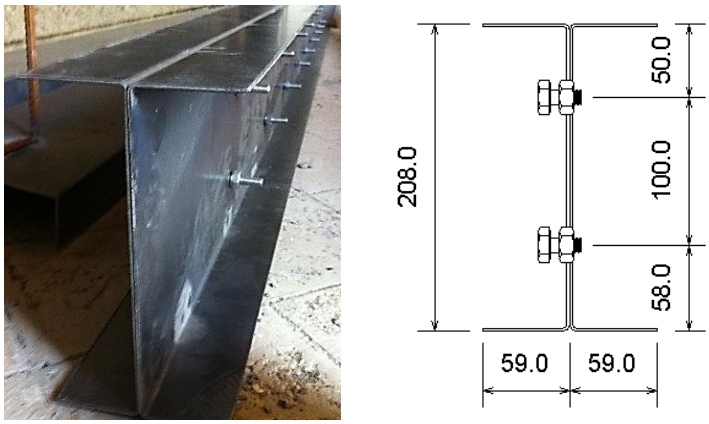

Figure 3. Built-up I section preparation

Figure 4. Wood stiffeners

Figure 5. Shear suds in the single channels model

For the second and fifth models, that have a shear studs, Since the steel sections are light gage and the welding of shear studs is not applicable [7], shear studs of 10mm in diameter have been drilled to the top flange as close as possible to the web to prevent the tear out of the flange before attaining full shear resisting strength see Figure 5. For the fifth model, that has double channels, the shear studs struggled about the web. Along beam span, six shear studs have been distributed within 1m from each end with a spacing of 150mm center to center. All studs have a length of 42.5 mm to be with the limits of AISC Specification (I8.2) the states "the length of the shear stud may not be less than 4 stud diameters".

The wood form was fabricated such that the inner clear dimensions are 3m length by 1m width and a depth of 0.075 m. The form surfaces of the first, second, fourth, and fifth models have been maintained at the same level with the top flange of the steel beams. For the third and sixth models they have located at 33mm below the top flanges of the steel beams.

Rebars with 10 mm diameter and a spacing of 200 mm have been used in both directions. The secondary or temperature rebars have length of 2950 mm while the main rebars have length of 950 mm. Spacers have been used to locate the main rebars at 33 mm above the wood form surface.

5. Concrete Casting and Curing

Several trial mixes were executed to get proportions of 1: 1.25: 1.75 and a water-cement ratio of 0.55 for a cube compressive strength of 35 MPa. The molds were lubricated with thin layer of oil, and then the concrete poured in the mold as indicated in Figure 6. A vibrator was used when necessary. Two cubical specimens were taken from each model and they were cured and tested at 28 days to ensure that the specified strength is achieved.

Figure 6. Concrete casting

6. Test Setup

All of the six models were supported and loaded in the same way. Beams of the models were simply supported with rollers at 0.075 m away from the ends. The concrete was dyed with a thin layer of white paint to make the cracks more visible and more traceable. The distribution beams were placed on the concrete surface at 1.0 m from the supports. A jack of 30 ton and load cell of 100 ton were installed at the mid-distance between the distribution beams as shown in Figure 7. Two dial gauges, one for the concrete and one for the steel, were attached at the mid-span to measure the displacement. Five strain gauges were installed at different locations in the mid span region. Two at top and bottom of concrete surface while the other three were at top and bottom of the flange and at the web of the steel section. These strain gauges measured the strains in the concrete slab, and in the steel sections.

Before attachment of the strain gages, the steel and concrete surfaces were firstly smoothened, polished, and cleaned; then the strain gauge were glued to ensure a perfect contact. The strain gauges were coated with a special coat indicated in Figure 8. Finally, the strain gauges were connected to the channels of the data logger.

The data logger has been manufactured locally to obtain accurate high-resolution strain measurements. It consists of quarter bridge (tension / compression) with 120 Ω resistance of strain. The data logger has been connected to a computer to display and record the results of the measured strains.

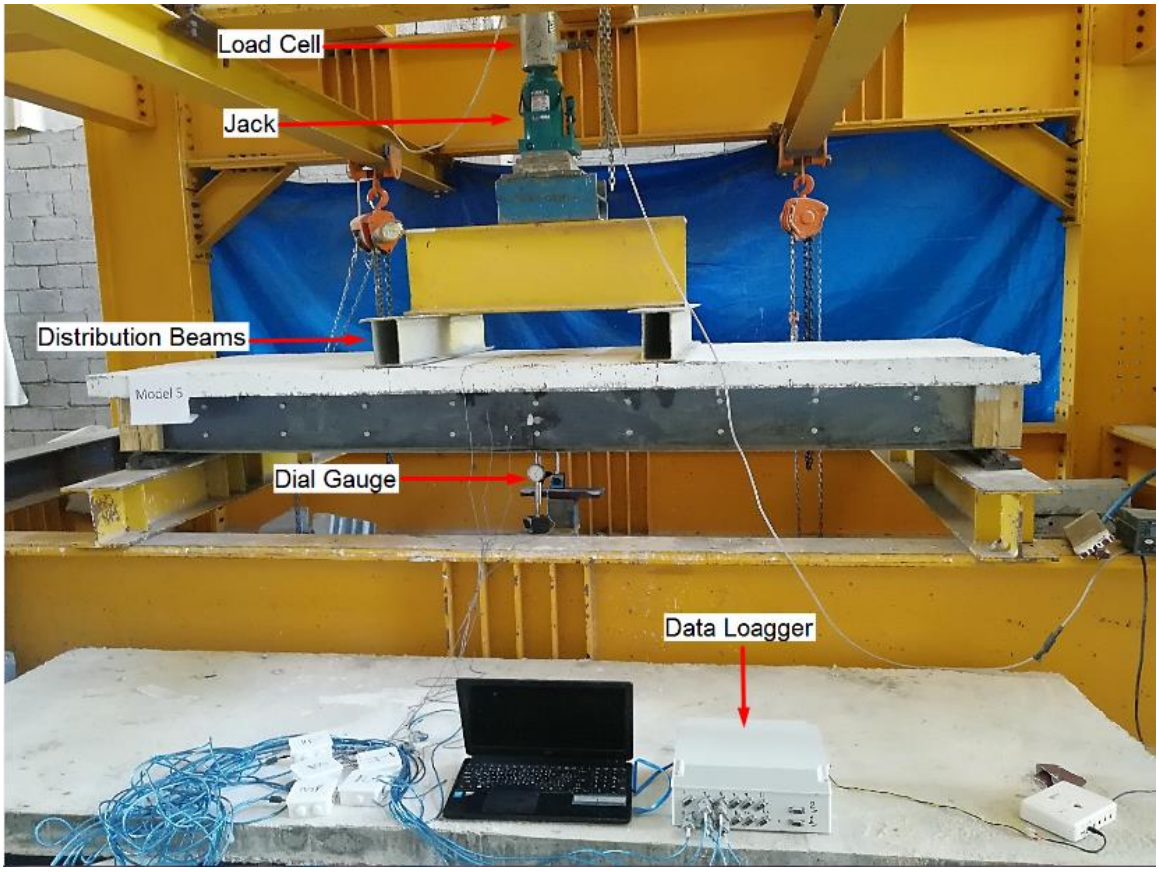

Figure 7. Test setting

Figure 8. Applying the strain gauges

7. Results and Discussion

7.1. Notations

For a more readable presentation of the results, symbols of M1 through M6 have been used to refer respectively to the first through the sixth model.

7.2. Concrete Compressive Strength

At the day of test, the cube specimens that prepared during the casting process have been tested and their compressive strengths have been presented in Table 5. Except batch M3 that mixed manually, all other batches have been mixed using a ready mixer. This may explain the relatively low compressive strength of the M3.

Table 5. Cubes compressive strength in MPa

Model Number	Average density (kg/m^3)	Average strength in (MPa)
M 1	2257	31.25
M 2	2301	26.09
M 3	2137	22.21
M 4	2372	35.96
M 5	2309	28.865
M 6	2309	34.99

7.3. Load-deflection Curves

During the tests, the applied load has been measured via the load cell for each increment while the corresponding mid-span vertical deflections have been measured using the dial gauges for the concrete and steel. Load -deflection curves for M1 through M6 have been respectively presented in Figure 9 through Figure 14. These figures show that:

- For the single channel models M1, M2, and M3; the load carrying capacity of the non-composite model M1 is 82.9% less than the capacity of the composite models M2 and M3. The models M2 and M3 almost have equal strength to indicate no significant difference between embedded of the flange or using shear studs to have the composite action.
- For the built-up models M4, M5, and M6; the load carrying capacity of the non-composite model M4 is 44.2 % less than the loads of the composite model M5 and 48.7% less than model M6. The load carrying capacity of model M5 is 8% less than that of M6 to indicate that the embedded flange composite action is more effective than that of the shear studs.
- A premature failure has been noted in M1. This may be due to some imperfection that have been noted during the casting and transformation processes.
- The models M2 and M3 that had an elastoplastic behavior shows that M2 beams reached a deflection about 50% less than obtained in M3.
- Regarding to the M4, a separation between the concrete and the top flange can be noted from Figure 12. This may explain the failure due to elastic buckling that prevents the subsequent elasto-plastic behavior. On the other hand, no separations have been noted in M5, and M6 which have elasto-plastic behavior.

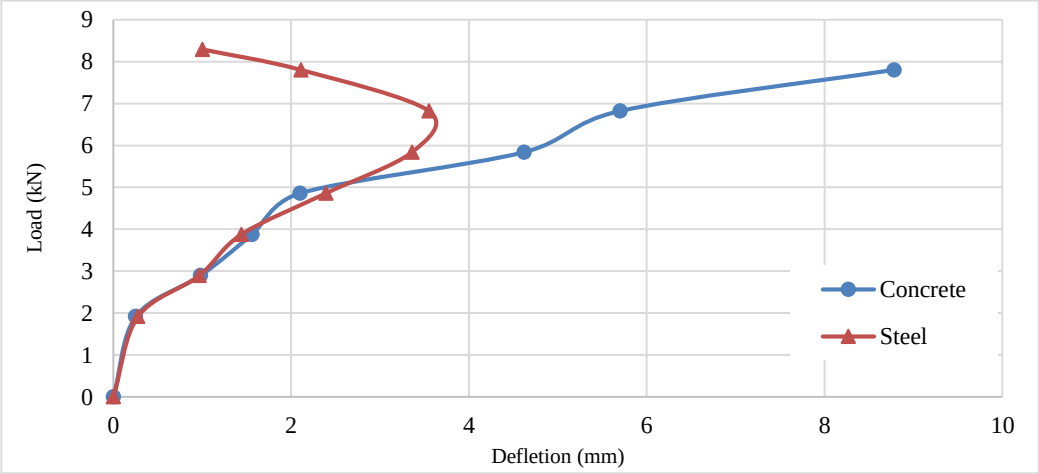

Figure 9. Load-deflection curve of M1

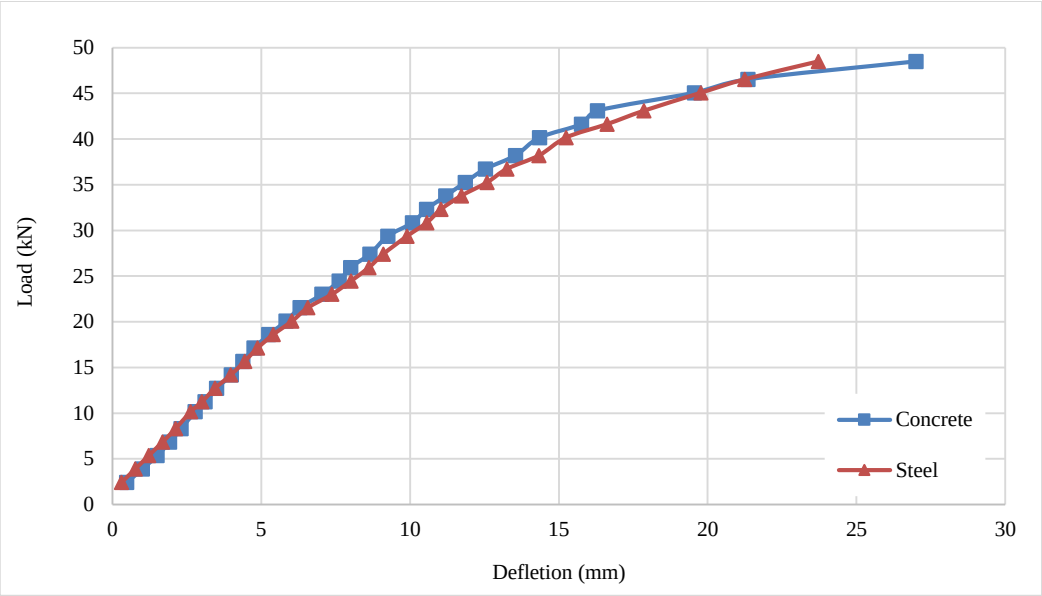

Figure 10. Load-deflection curve of M2

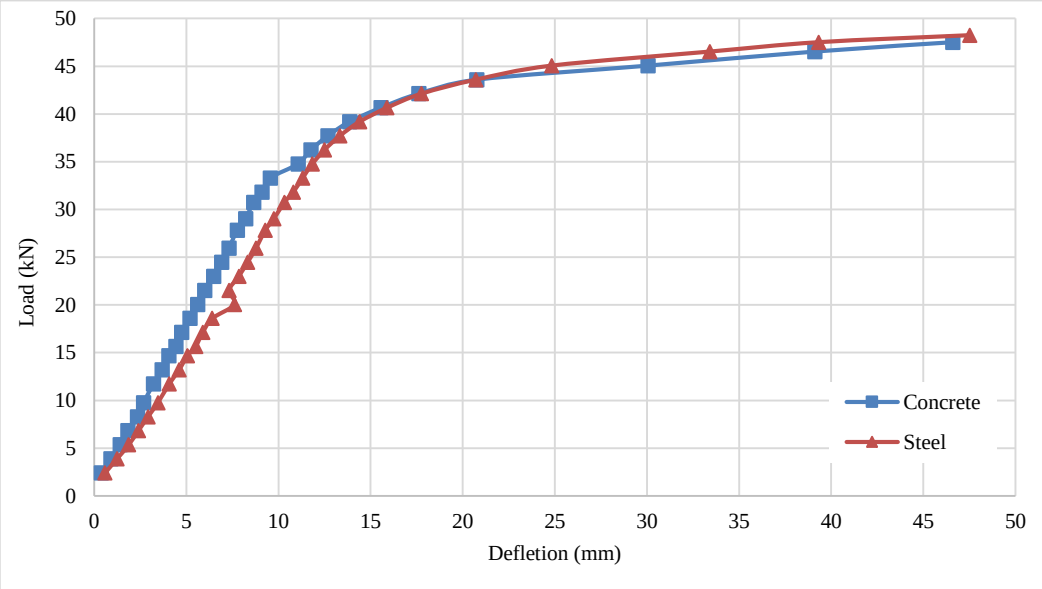

Figure 11. Load-deflection curve of M3

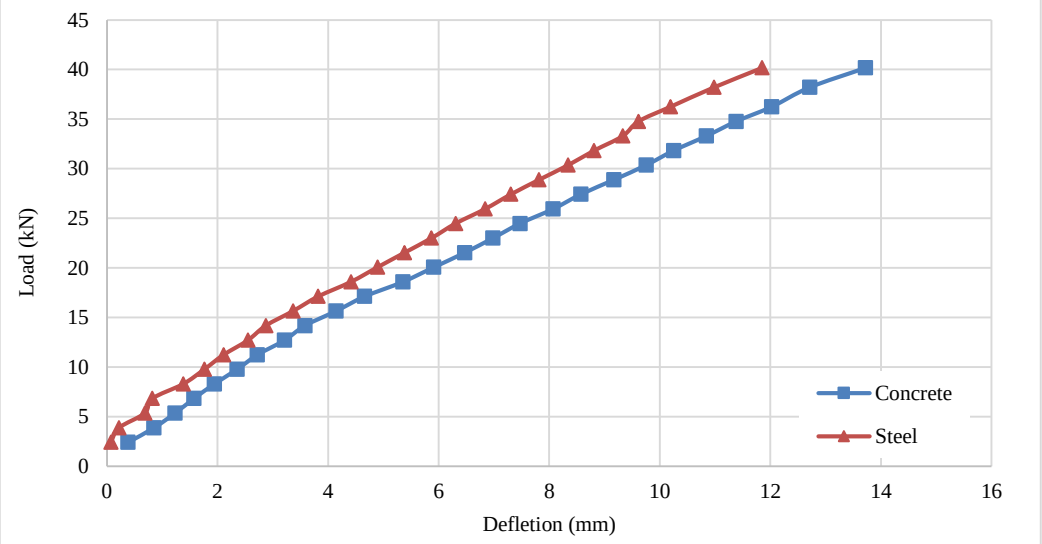

Figure 12: Load-deflection curve of M4

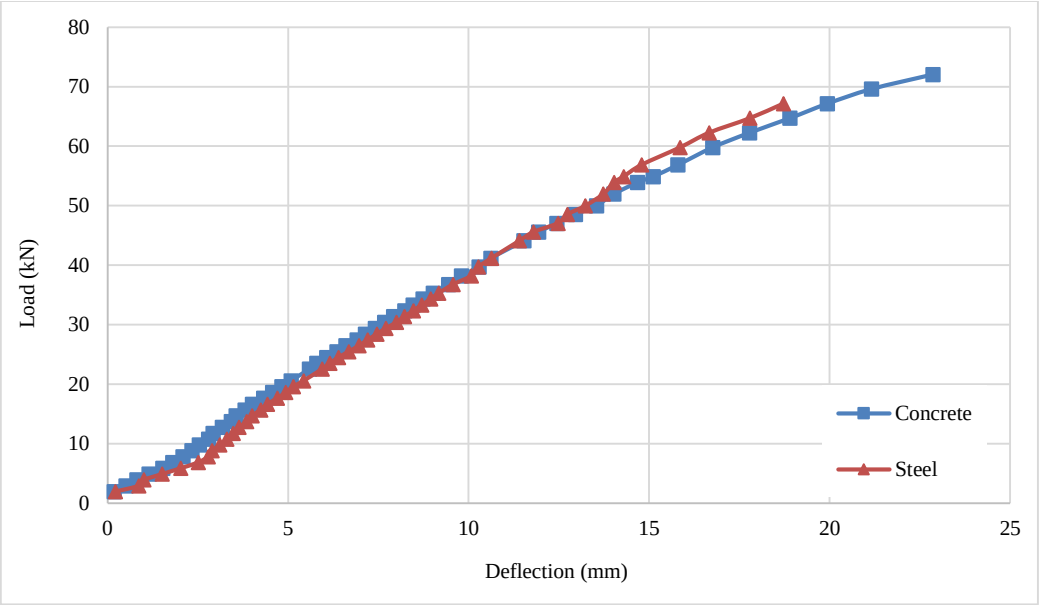

Figure 13. Load-deflection curve of M5

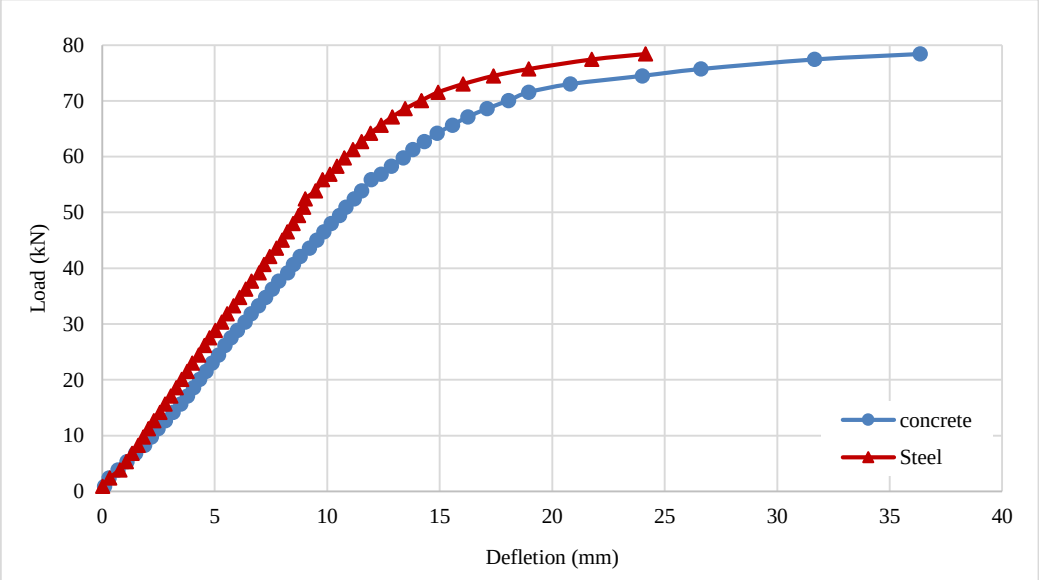

Figure 14. Load-deflection curve of M6

7.4. Load-strain Curves of the Steel Beams

Beams mid-span strains have been measured at the web, the top flange, and the bottom flange for each load increment and they have been presented in the load-strain curves of Figure 15 through Figure 20 for M1 through M6 respectively. In these curves, the positive sign indicates a compressive strain and vice versa. From these curves, one may note that:

- For the non-composite models M1 and M4, the neutral axis is located in the beam web. Strains for M1and M4 are below the yield strain to indicate that the beam has a premature failure.
- For the models M2 and M5, that have shear studs, the stains indicate the top flange exposes to a tensile strain at the initial stage of loading then the neutral axis is settled below the top flange and. Both M2 and M5 bottom flanges reached to the yield strain before the failure.
- In the failure of the embedded flanges models M3 and M6 the bottom flanges and the web reached at strain more than 0.008. For the M3the top flanges expose to tension as the neutral axis is above the top flange, but for M6 the top flange is expose to compression.

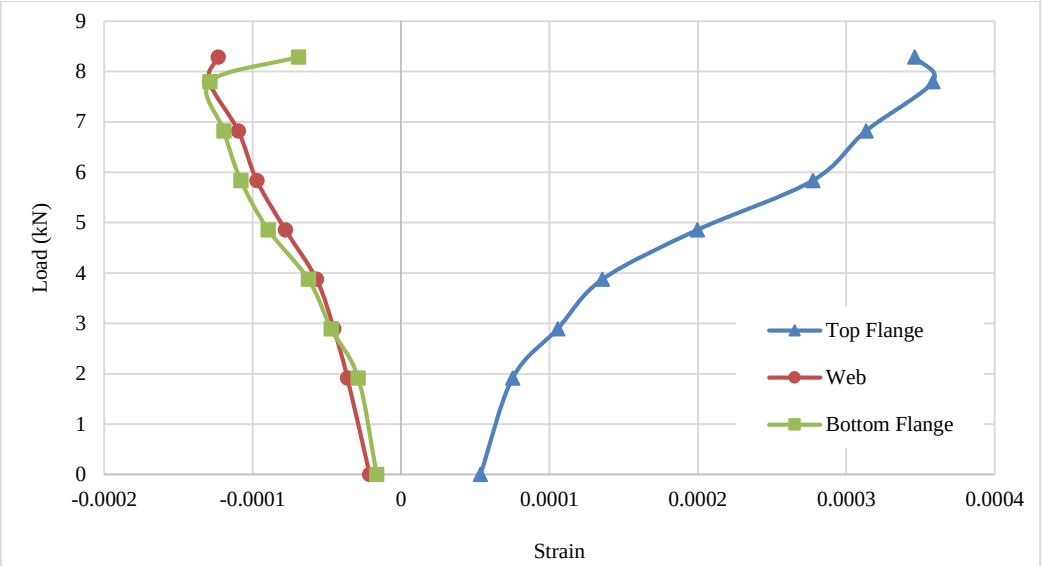

Figure 15. Load-strain curve of steel beams in M1

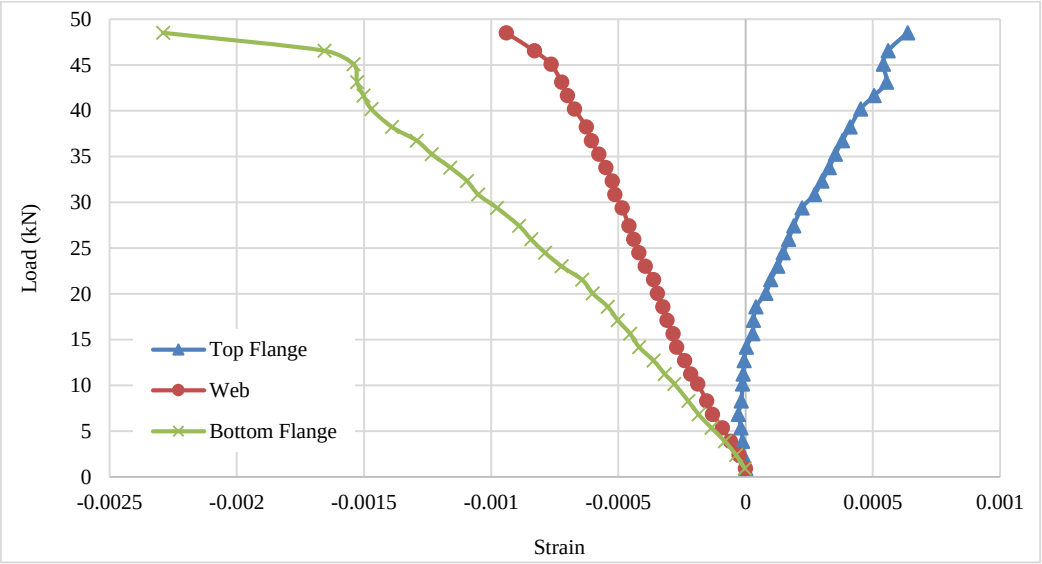

Figure 16. Load-strain curve of steel beams in M2

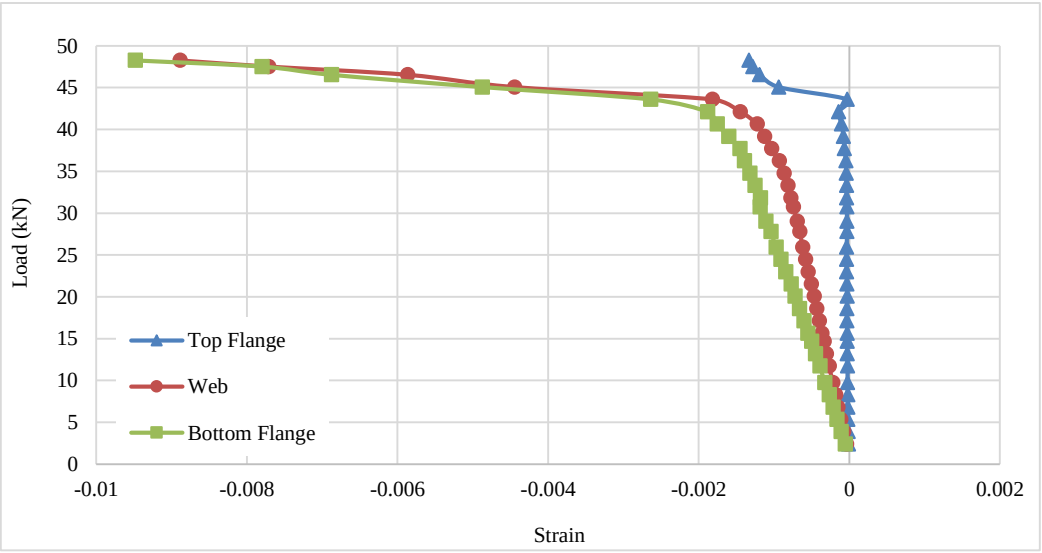

Figure 17. Load-strain curve of steel beams in M3

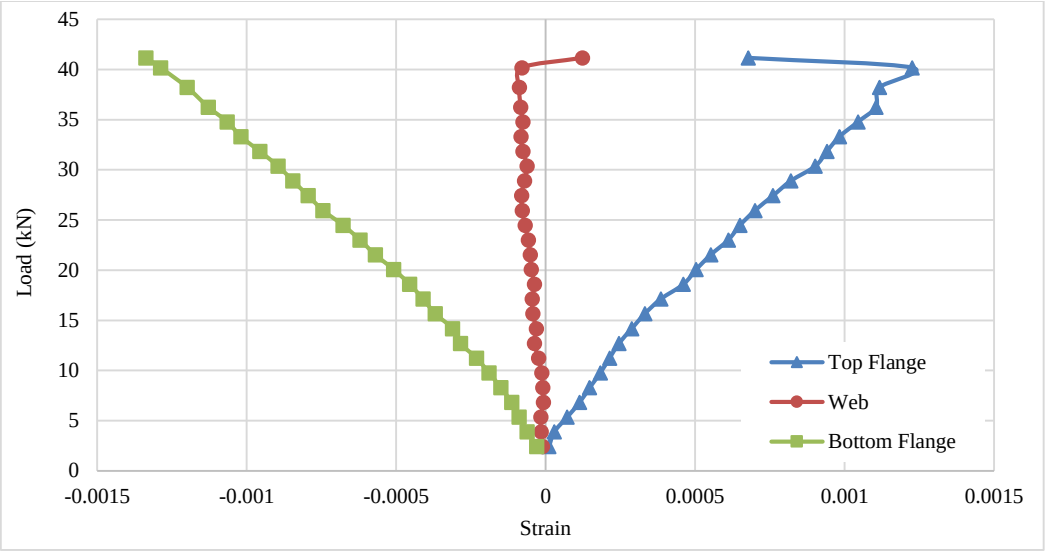

Figure 18. Load-strain curve of steel beams in M4

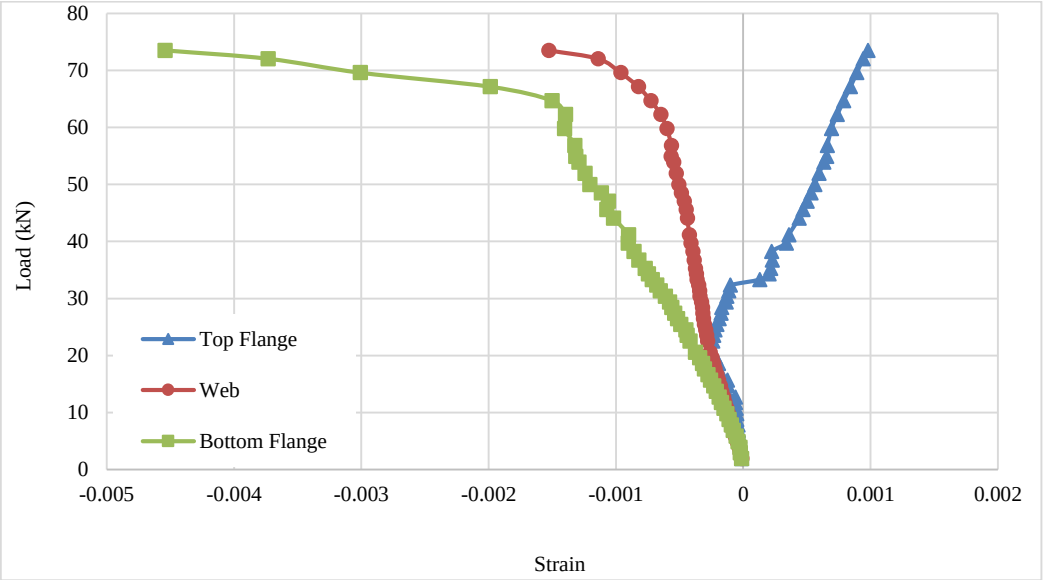

Figure 19. Load-strain curve of steel beams in M5

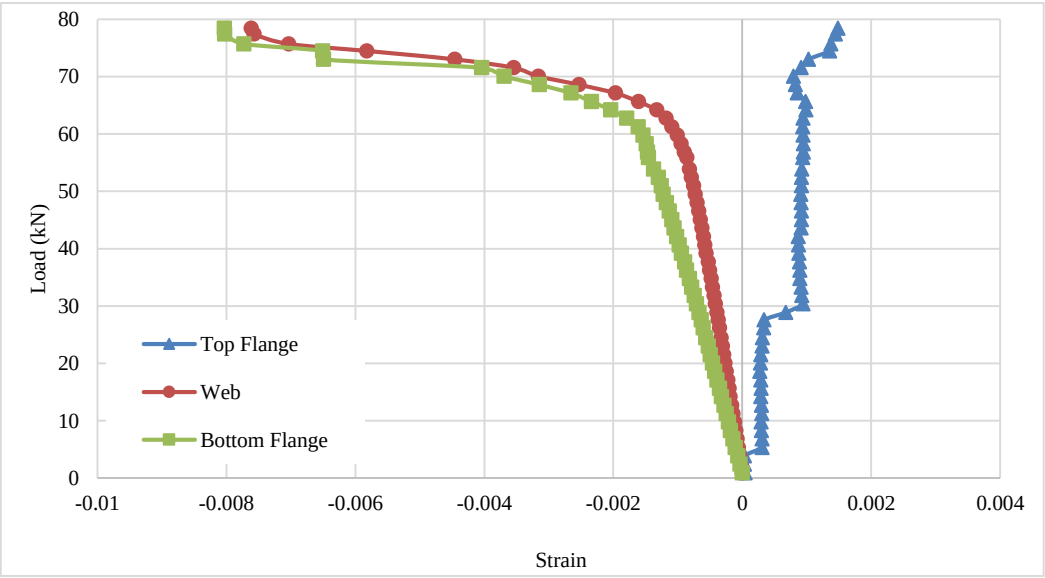

Figure 20. Load-strain curve of steel beams in M6

7.5. Load-strain Curves for Concrete

As discussed previously, gauges have been attached to the top and bottom of the slab to measure the stain of the concrete at the mid-span for each load increment to determine the load-strain curves. These curves for M1 through M6 have been respectively presented in Figure 21 through Figure 26. During the test of M1 and M2, the bottom flange strain gauges have been damaged and could not repaired so, their results have been excluded. The results show that:

- M1, M2 the strain at the top surface was increasing until it reached to about 0.0004 and then it starts to decrease. When the steel beams laterally buckle, the concrete slab will drop and support smaller loads and the strains are correspondingly recover as indicated.
- M3, M4, and M5 show that the maximum concrete strain is in the range of 0.001 when the failure occurs in the steel beams. The concrete top surface is subjected to a compression stresses while the bottom surface is subjected to a tension stress.
- The bottom concrete surface of M6 is subjected to a compression stress and the neutral axis is located in the web of steel beams below the concrete.

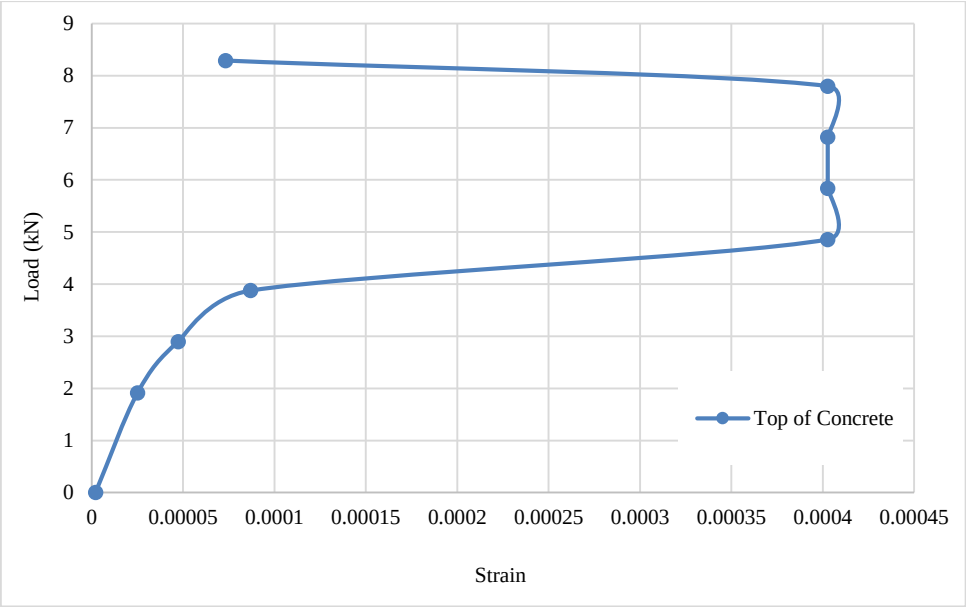

Figure 21. Load-strain curve of concrete in M1

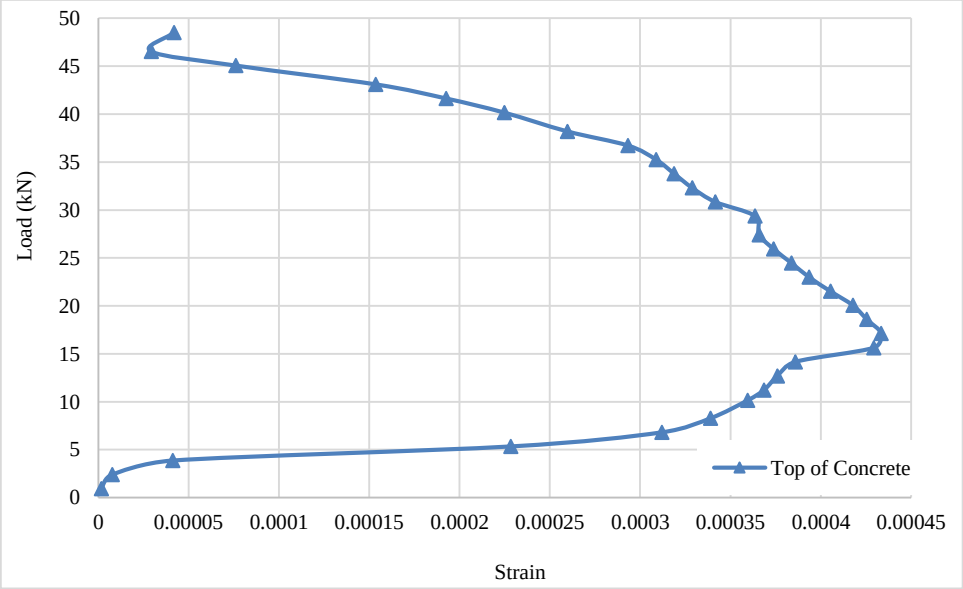

Figure 22. Load-strain curve of concrete in M2

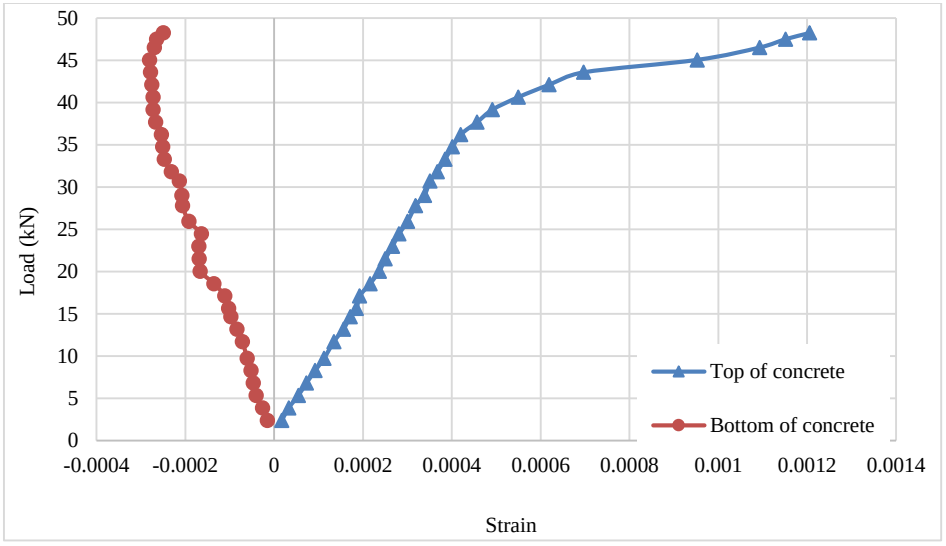

Figure 23. Load-strain curve of concrete in M3

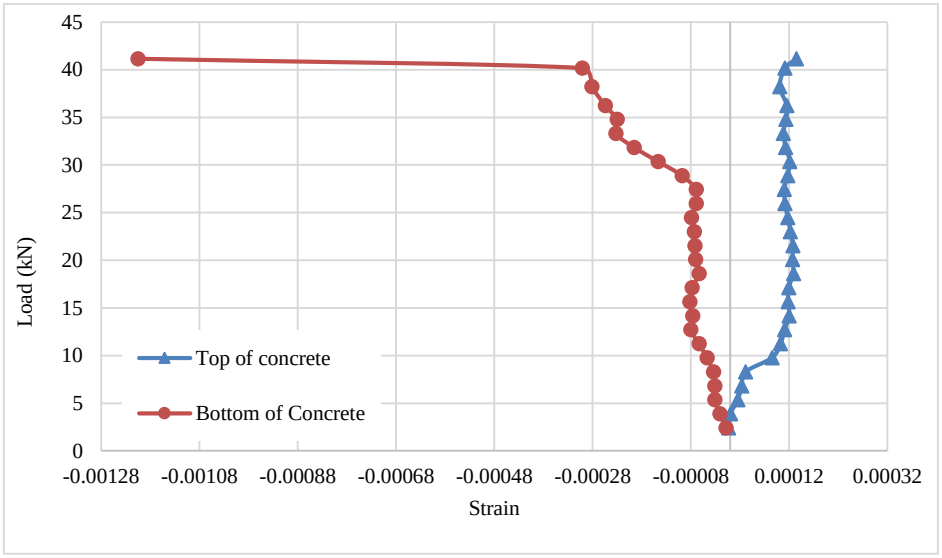

Figure 24. Load-strain curve of concrete in M4

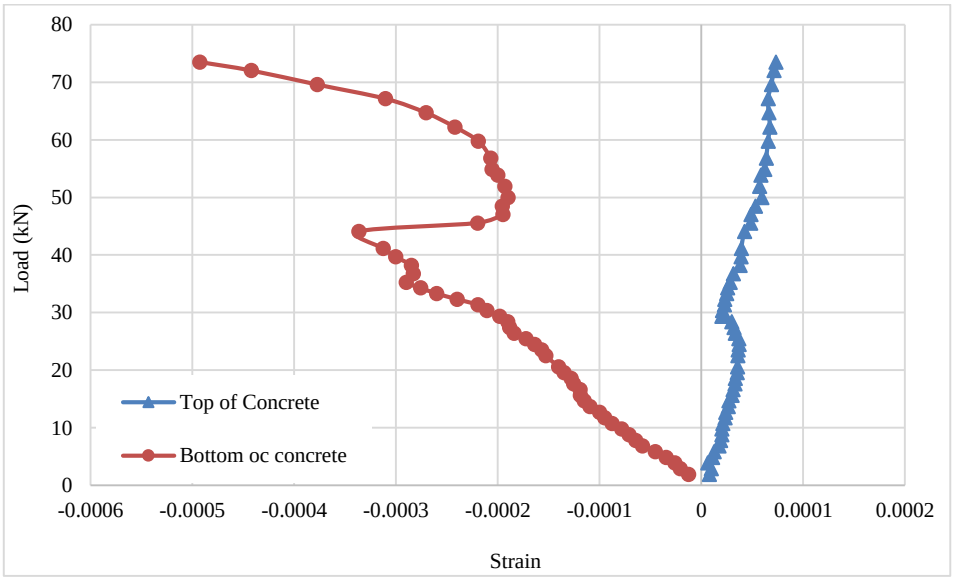

Figure 25. Load-strain curve of concrete in M5

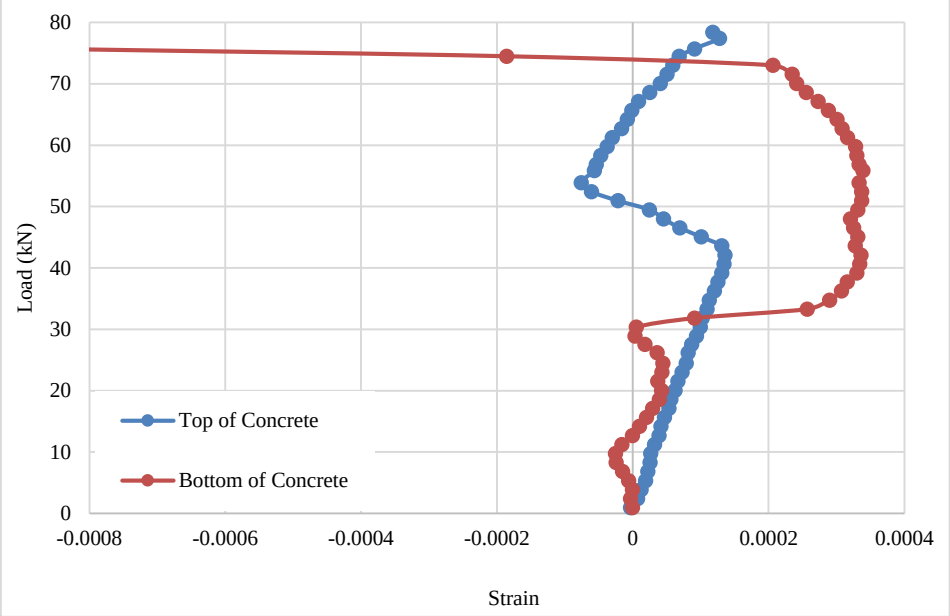

Figure 26. Load-strain curve of concrete in M6

7.6. Failure Modes

A premature failure mode was noted in M1. This may be due to the imperfection in the steel beams that have been noted during the casting and transformation processes. The failure mode was a global buckling mode and the steel beams were separated from the concrete as indicated in Figure 27. For M2, the failure load was about 48kN and the failure mode was a global buckling as indicated in Figure 28 with no separation between the concrete and steel beams. Regarding to M3, the failure load was equal to 48kN with an excessive concrete deflection of 47mm as indicated in Figure 29, tension cracks started to appear at load 20 kN. The failure mode was a global one. The failure load of M4 was close to 40kN with a local buckling at loading points. At the ends, separation indicated in Figure 30 has been noted. For M5, a global buckling mode indicated in Figure 31 has been noted at a failure load of 72 kN. Finally, the failure mode of M6 was a local buckling mode where the flanges locally buckled at the supports as indicated in Figure 32 at a load 78 kN. In all the models miner cracks was observed in the concrete slab in the pure bending zone.

Figure 27. Failure mode of M1

Figure 28. Failure mode of M2

Figure 29. Failure mode of M3

Figure 30. Failure mode of M4

Figure 31. Failure mode of M5

Figure 32. Failure mode of M6

8. Conclusions

Six models have been tests to investigate the behavior of non and partially composite cold-formed steel beams of different connection. The following conclusions may be pointed:

- Except the fourth and the sixth models that failed in local buckling modes, all other models failed in global lateral-torsional buckling modes
- For a single C-channel beams the load carrying capacity of the first model non-composite model is 82.9% less than the capacity of the composite models. The strength of the second and the third model are almost equal indicating that no significant difference between embedded of the flange or using shear studs to have the composite action.
- For the built-up models the load carrying capacity of the non-composite model is 44.2 % less than the loads of the fifth model and 48.7% less than the sixth model. The load carrying capacity of the fifth model is 8% less than that of the sixth model to indicate that the embedded flange composite action is slightly more effective than that of the shear studs.
- A premature failure has been noted in first model. This may be due to some imperfection that have been noted during the casting and transformation processes. The second and third models that had an elasto-plastic behavior shows that the beams of the second model reached a deflection about 50% less than that obtained in the third model.
- The fourth model shows a separation between the concrete and the top flange. This may explain the failure due to elastic buckling that prevents the subsequent elasto-plastic behavior. On the other hand, no separations have been noted in the fifth and sixth model which have elasto-plastic behavior.
- For the non-composite models, the neutral axis is located in the beam web. Beam strains are below the yield strain to indicate that the beam has a premature failure. For the models that have shear studs, the beam stains indicate the top flange exposes to a tensile strain at the initial stage of loading. Both models bottom flanges reached to the yield strain before the failure. The failure of the embedded flanges models the bottom flanges and the web reached at strain more than 0.008.
- The strain at the top surface of concrete of the first and second model was increasing until it reached to about 0.0004 and then it starts to decrease. When the steel beams laterally buckle, the concrete slab will drop and support smaller loads and the strains are correspondingly decreases.
- The maximum concrete strain in the third, fourth, and fifth model was in the range of 0.001 when the failure occurs in the steel beams. The concrete top surface is subjected to a compression stresses while the bottom surface is subjected to a tension stress.
- The bottom concrete surface of the sixth model was subjected to a compression stress and the neutral axis is located in the web of steel beams below the concrete.

9. Conflict of Interest

The authors declare no conflict of interest.

10. Funding

This work supported by the laboratories of Baghdad University, Baghdad, Iraq.

11. References

[1] Put, Bogdan M., Yong-Lin Pi, and N. S. Trahair. "Lateral Buckling Tests on Cold-Formed Channel Beams." Journal of Structural Engineering 125, no. 5 (May 1999): 532–539. doi:10.1061/(asce)0733-9445(1999)125:5(532).

[2] Pi, Yong-Lin, B. M. Put, and N. S. Trahair. "Lateral Buckling Strengths of Cold-Formed Channel Section Beams." Journal of Structural Engineering 124, no. 10 (October 1998): 1182–1191. doi:10.1061/(asce)0733-9445(1998)124:10(1182).

[3] Dolamune Kankanamge, Nirosha, and Mahen Mahendran. "Behaviour and Design of Cold-Formed Steel Beams Subject to Lateral–torsional Buckling." Thin-Walled Structures 51 (February 2012): 25–38. doi:10.1016/j.tws.2011.10.012.

[4] Anbarasu, M. "Local-Distortional Buckling Interaction on Cold-Formed Steel Lipped Channel Beams." Thin-Walled Structures 98 (January 2016): 351–359. doi:10.1016/j.tws.2015.10.003.

[5] Wang, Liping, and Ben Young. "Behaviour and Design of Cold-Formed Steel Built-up Section Beams with Different Screw Arrangements." Thin-Walled Structures 131 (October 2018): 16–32. doi:10.1016/j.tws.2018.06.022.

[6] Hadjipantelis, Nicolas, Leroy Gardner, and M. Ahmer Wadee. "Prestressed Cold-Formed Steel Beams: Concept and Mechanical Behaviour." Engineering Structures 172 (October 2018): 1057–1072. doi:10.1016/j.engstruct.2018.06.027.

[7] Hanaor, Ariel. "Tests of Composite Beams with Cold-Formed Sections." Journal of Constructional Steel Research 54, no. 2 (May 2000): 245–264. doi:10.1016/s0143-974x(99)00046-2.

[8] Lakkavalli, Bhavani Shankar, and Yi Liu. "Experimental Study of Composite Cold-Formed Steel C-Section Floor Joists." Journal of Constructional Steel Research 62, no. 10 (October 2006): 995–1006. doi:10.1016/j.jcsr.2006.02.003.

[9] Xu, L., and F.M. Tangorra. "Experimental Investigation of Lightweight Residential Floors Supported by Cold-Formed Steel C-Shape Joists." Journal of Constructional Steel Research 63, no. 3 (March 2007): 422–435. doi:10.1016/j.jcsr.2006.05.010.

[10] Kyvelou, Pinelopi, Leroy Gardner, and David A. Nethercot. "Composite Action Between Cold-Formed Steel Beams and Wood-Based Floorboards." International Journal of Structural Stability and Dynamics 15, no. 08 (December 2015): 1540029. doi:10.1142/s0219455415400295.

[11] Kyvelou, Pinelopi, Leroy Gardner, and David A. Nethercot. "Testing and Analysis of Composite Cold-Formed Steel and Wood−Based Flooring Systems." Journal of Structural Engineering 143, no. 11 (November 2017): 04017146. doi:10.1061/(asce)st.1943-541x.0001885.

[12] Kyvelou, Pinelopi, Leroy Gardner, and David A. Nethercot. "Finite Element Modelling of Composite Cold-Formed Steel Flooring Systems." Engineering Structures 158 (March 2018): 28–42. doi:10.1016/j.engstruct.2017.12.024.

[13] Fratamico, David C., Shahabeddin Torabian, Xi Zhao, Kim J.R. Rasmussen, and Benjamin W. Schafer. "Experimental Study on the Composite Action in Sheathed and Bare Built-up Cold-Formed Steel Columns." Thin-Walled Structures 127 (June 2018): 290–305. doi:10.1016/j.tws.2018.02.002.

[14] Fiorino, Luigi, Vincenzo Macillo, and Raffaele Landolfo. "Experimental Characterization of Quick Mechanical Connecting Systems for Cold-Formed Steel Structures." Advances in Structural Engineering 20, no. 7 (September 30, 2016): 1098–1110. doi:10.1177/1369433216671318.

[15] Ungureanu, Viorel, Maria Kotełko, Anna Karmazyn, and Dan Dubina. "Plastic Mechanisms of Thin-Walled Cold-Formed Steel Members in Eccentric Compression." Thin-Walled Structures 128 (July 2018): 184–192. doi:10.1016/j.tws.2017.09.029.

[16] Sena Cardoso, Francisco, Hao Zhang, Kim J.R. Rasmussen, and Shen Yan. "Reliability Calibrations for the Design of Cold-Formed Steel Portal Frames by Advanced Analysis." Engineering Structures 182 (March 2019): 164–171. doi:10.1016/j.engstruct.2018.12.054.

[17] Yao, Ye, Wai-Meng Quach, and Ben Young. "Finite Element-Based Method for Residual Stresses and Plastic Strains in Cold-Formed Steel Hollow Sections." Engineering Structures 188 (June 2019): 24–42. doi:10.1016/j.engstruct.2019.03.010.

[18] Kyvelou, Pinelopi, Leroy Gardner, and David A. Nethercot. "08.09: Design of Cold-Formed Steel Composite Flooring Systems with Partial Shear Connection." Ce/papers 1, no. 2–3 (September 2017): 1899–1908. doi:10.1002/cepa.234.